J. Min. Metall. Sect. B-Metall. 51 (1) B (2015) 81 - 87

Journal of Mining and Metallurgy, Section B: Metallurgy

MECHANICAL PROPERTIES OF LOW ALLOY HIGH PHOSPHORUS WEATHERING STEEL

B.K. Jena [a], N. Gupta [b], B. Singh [c], G. Sahoo [c,*]

[a] Dr B R Ambedkar Institute of Technology, Port Blair, A&N Islands, India
[b] National Institute of Foundry & Forge Technology, Hatia, India
[c] R & D Centre for Iron and Steel, SAIL, Doranda, India

(Received 20 January 2014; accepted 27 October 2014)

Abstract

Mechanical behaviour of two low alloy steels (G11 and G12) was studied with respect to different phosphorus contents. Tensile strength and yield strength increased while percentage elongation at fracture decreased on increasing phosphorus content. The SEM and light optical photomicrograph of low phosphorus steel (G11) revealed ferrite and pearlite microstructures. On increasing phosphorus content from 0.25 wt.% to 0.42 wt.%, the morphology of grains changed from equiaxed to pancake shape and grain size also increased. The Charpy V notch (CVN) impact energy of G11 and G12 steel at room temperature was 32 J and 4 J respectively and their fractographs revealed brittle rupture with cleavage facets for both the steels. However, the fractograph of G11 steel after tensile test exhibited ductile mode of fracture with conical equiaxed dimples while that of G12 steel containing 0.42 wt. % P exhibited transgranular cleavage fracture. Based on this study, G11 steel containing 0.25 wt. % P could be explored as a candidate material for weathering application purpose where the 20 ^{o}C toughness requirement is 27 J as per CSN EN10025-2:2004 specification.

Keywords: Strengths; Steel; Mechanical Properties; Phosphorus.

1. Introduction

Weathering steel has potential application in civil engineering and transportation application. The various structural applications include bridges, guard rails, buildings, power poles, transmission towers etc. The weathering steel normally, composed of small amount of alloying elements e.g. Cr, Cu, Ni and P etc [1-5] which promotes formation of a stable protective rust layer. Especially, the effect of phosphorus on weathering properties is well known. The 1600-year old Delhi Iron Pillar is a living example for its remarkable corrosion resistance. The presence of relatively high phosphorus content (0.25 wt %) in the pillar plays a major role by facilitating the formation of a protective passive film on the surface [6, 7]. As reported by G P Zhou et.al [8], the rust became more homogeneous and compact on increasing P content in cast strips. The P enrichment was observed at the interface between rust layer and substrate, which was believed to be responsible for the improvement of weathering resistance by retarding ingress of aggressive ions and moisture.

On the other hand, the effect of phosphorus in steel is considered as detrimental on the mechanical properties due to its grain boundary segregation. Phosphorus in steel also exhibits temper embrittlement during prolonged exposure or when slowly cooled in the temperature range of 250-650^{0} C [9-11]. In this temperature range, phosphorus segregates to grain boundary preferentially and decreases grain boundary cohesive energy, which leads to a tendency for intergranular brittle fracture. The embrittlement effect of phosphorus manifests itself by change in the brittle fracture mode from cleavage to intergranular mode; decrease in impact energy and by rise in ductile-to-brittle transition temperature (DBTT) [12].

The presence of small amount of carbon displaces phosphorus from grain boundaries by site competition effect [13, 14]. Carbon in the range 0.01-0.05 wt % improves grain boundary cohesion [13]. Abiko et.al [13] and Suzuki et.al [14] determined that the optimum value of carbon concentration in obtaining ductile fracture in high purity Fe-P steel was 0.01 wt %. Addition of low amount of boron in the range of 12.5 ppm to Fe-P steel has been also beneficial in reducing grain boundary segregation of phosphorus and decreasing ductile to brittle transition temperature [15-17]. Two hypotheses have been proposed for explaining the effect of boron on enhancing grain boundary cohesion in steel [17]. According to the first hypothesis, grain boundary cohesion is caused by boron itself as its intrinsic effect when it segregates to grain boundary. The other proposition is that boron

* *Corresponding author: gadadhar@sail-rdcis.com*

DOI:10.2298/JMMB140120005J

Table 1. *Chemical compositions (wt %) of the investigated steels G11 and G12*

Sl No	samples	C	Si	Mn	S	P	B	Cr	Cu	Ni	Al
1	G-11	0.085	0.085	0.24	0.009	0.25	0.0022	0.36	0.3	0.2	0.02
2	G-12	0.085	0.09	0.28	0.007	0.42	0.0022	0.36	0.3	0.2	0.011
3	LC	0.086	0.11	0.29	0.01	-	-	-	-	-	0.03

suppresses phosphorus segregation by a site competition effect where phosphorus is replaced by boron at grain boundaries. Therefore, addition of boron in small amount may improve mechanical properties of high phosphorus containing steels.

This study was mainly intended to evaluate the mechanical properties of high phosphorus containing boron added low alloy steels to be used for structural applications.

2. Experimental

2.1 Material

Heats of low alloy steels of 25 kg each were made utilizing a high frequency induction-melting furnace of 100 kg capacity. Steel scraps of C-Mn rail steel had been added to soft iron (0.001 wt. % C) to balance carbon content. In order to obtain Cr, P, Cu and Ni in the desired range, Fe-P and Fe-Cr mother alloys, Cu blocks and Ni lumps were added to the liquid steel in the furnace. The melts were cast into ingots of cross sectional dimensions 100mm × 100mm. Subsequently, the ingots were hot rolled in two stages. In first stage, the ingots were rolled into 16 mm thickness plates through five passes after soaking at 1150^{o}C for 2.5 hours. The finishing temperature was about 950^{0}C. In the second stage, once again these plates were soaked for 30 min at 1150^{0}C and hot rolled into 5 mm thickness plates through three passes. The finishing temperature was about 800 to 830^{0}C. Chemical compositions of each steel was determined using an Optical Emission Spectrometer and provided in Table-1. All the composition reported in this paper is in wt.%. Heat of a low carbon steel (LC) was also made for comparison purpose.

2.2 Microscopy

Specimens (20mm×15mm×5mm) for metallography study were grounded successively to 1200 grit water proof SiC paper followed by cloth polishing using alumina suspension. Subsequently, the specimens were microscopically examined using a Scanning Electron Microscope (EVO MA 10, Carl Zeiss) after etching with 2 % Nital. A light optical microscope (Model: LEICA DMRME) and Lieca MW software were used for measuring grain size and volume fraction. The measurement was carried out atleast at four different fields.

2.3 Mechanical test

Tensile test was conducted on the standard flat samples of gauge length 50 mm as per ASTM E 8M-98 [18]. The testing was performed in triplicate at room temperature using universal testing machine, UTM-7200 (Dak System Inc.) with a cross head speed of 2mm/min and the corresponding strain rate of 6.67×10^{-4} s^{-1} as per the requirement of static tensile test. The fracture mode and morphology of the surface after tensile testing was examined using Scanning Electron Microscope, EVO MA 10, Carl Zeiss. In order to evaluate Charpy V-notch (CVN) energy, impact test was carried out on standard samples of dimension 55mm×10mm×10mm (Fig. 1) as per specification of ASTM E 23-05 [19]. The tests were conducted at room temperature in triplicate using a pendulum impact tester (TINIUS OLSEN WILLOW GROVE PA-USA). Similar to the fractography of tensile test specimens, the fractured surface of samples after impact test was also examined under Scanning Electron Microscope.

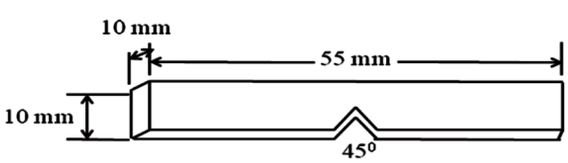

Figure 1. *Standard V-notched sample used for impact test according to ASTM E 23-05*

3. Result and Discussion

3.1 Microstructure

The light optical photomicrograph of G11 and G12 steels along cross section are shown in Fig. 2(a) and Fig. 2(b) respectively. The typical scanning electron micrograph along rolling direction of G11 steel is shown in Fig. 3(a) and (b) while that of G12 steel is shown in Fig. 3(c) and (d). Both light optical and SEM photomicrographs of G11 and G12 steel reveal ferrite and pearlite microstructure. While the microstructure of G11 steel shows equiaxed ferrite grains that of G12 steel shows pancake shaped grains. Furthermore, unlike G12 steel, the microstructure of G11 steel reveals uniform distribution of ferrite and pearlite. The average ferrite grain size of G12 steel is higher (13.98 mm) than that of G11 steel (11.27 mm) and the corresponding grain size distributions are 3 to

32 mm and 3 to 45 mm, respectively. On the other hand, the volume fraction of pearlite in G12 steel (6.46 ± 0.10) is lower than that of G11 steel (7.08 ± 0.16). These changes in microstructure are attributed to the influence of the phosphorus. As shown in the binary Fe-P phase diagram in Fig. 4(a), phosphorus acts as ferrite stabilizer and hence form a gama loop. Fig. 4(b) shows phase diagram of Fe-P system containing 50 ppm N with other elements as present in G11 steel. For G11 steel (0.25 % P), the finish rolling temperature (~950^{0}C) is above the g to (α+g) boundary line. In the case of G12 steel (0.42 % P), the the g to (α+g) boundary has been shifted to higher temperature. Therefore, on increasing phosphorus content may increase no recrystallization temperature (T_{nr}) of steel, which is the temperature below which no recrystallization takes place. These deformed grains will transform to ferrite along with grain refinement. However, as reported by Sahoo and Balasubramaniam [20], the complete homogenization of phosphorus of a Fe-0.32% P steel, cooled from (α+g) dual phase region, takes place after 16 hrs of soaking in ferrite region (900^{0}C), which shows that the diffusivity of phosphorus is very slow. Therefore, a displacive phase transformation type mechanism may be proposed in high phosphorus containing steel due to which all individual deformed austenite grains will transform completely to ferrite resulting in elongated grains as in the case of G12 steel (0.42 % P). Thus, increasing phosphorus content may lead to the formation of pancake shaped deformed grains along with increase in grain size.

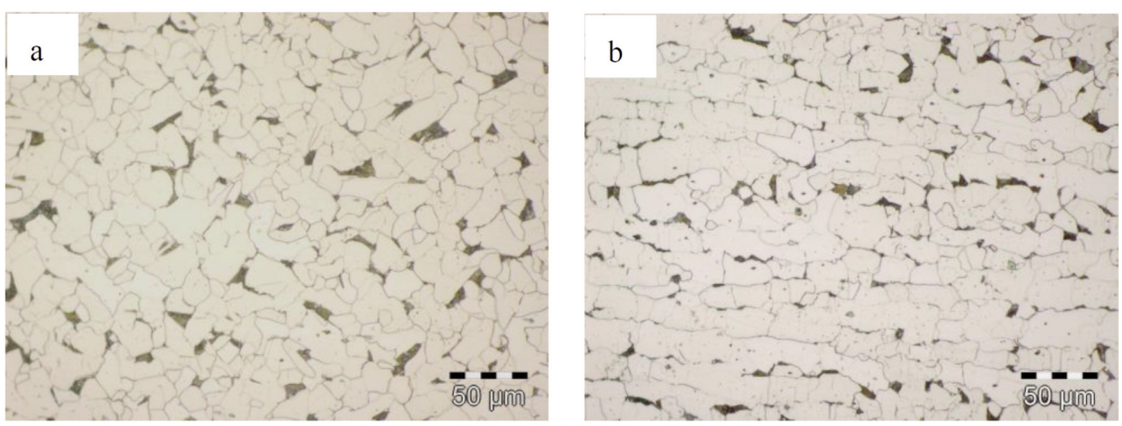

Figure 2. *Light optical photomicrograph of hot rolled steel: (a) G11 and (b) G12 along cross section*

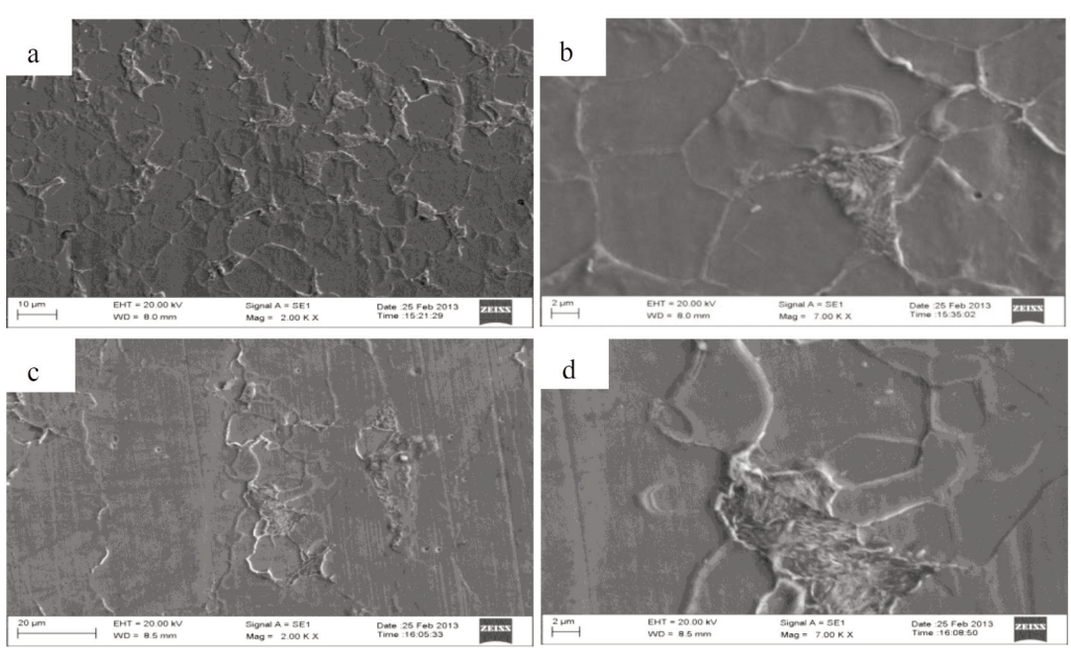

Figure 3. *SEM photomicrograph of as rolled G11 (a & b) and G12 (c &d) in lower and higher magnification along rolling direction*

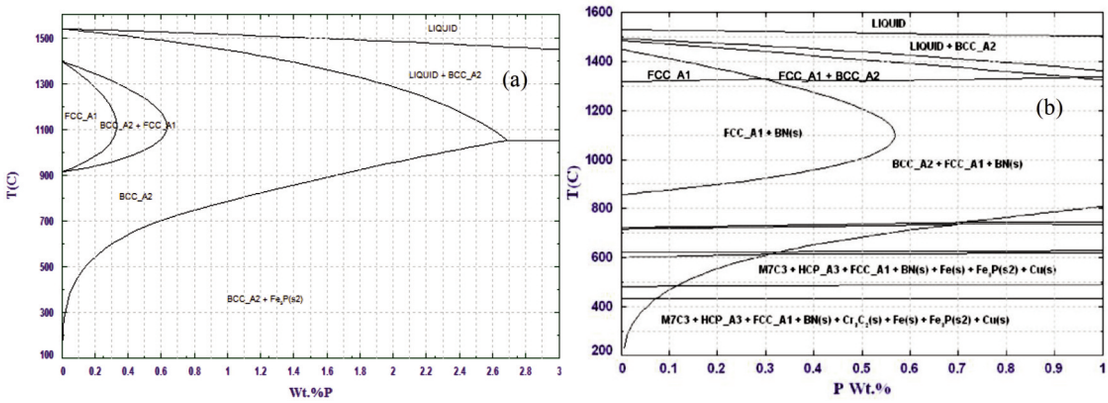

Figure 4. *Phase diagrams calculated using FactSage software for binary (a) Fe-P system and (b) Fe-P system with other elements as present in G11 steel and 50 ppm N.*

3.2 Mechanical Properties

Fig. 5 shows the typical engineering stress-strain curves of G11, G12 and LC steels. The yield point phenomenon has been observed in the phosphorus containing specimens, i.e. G11 (0.25 wt % P) & G12 (0.42 wt % P) steels due to the presence of interstitial elements like carbon and nitrogen. During plastic deformation, dislocations are locked due to the presence of these interstitial solute atoms and dislodging of these pinned dislocations resulted in yield point phenomena [21]. Although phosphorus is undesirable in modern steel making practices due to the poor mechanical properties, the typical engineering stress-strain curves of G11 and G12 resembles with that of low carbon steel (Fig. 5), especially with sufficient ductility. The mechanical properties (yield strength, ultimate tensile strength and percentage elongation at fracture) determined using extensometer are provided in the Table 2. The error bars in bar diagrams (Fig. 6) of YS, UTS, and

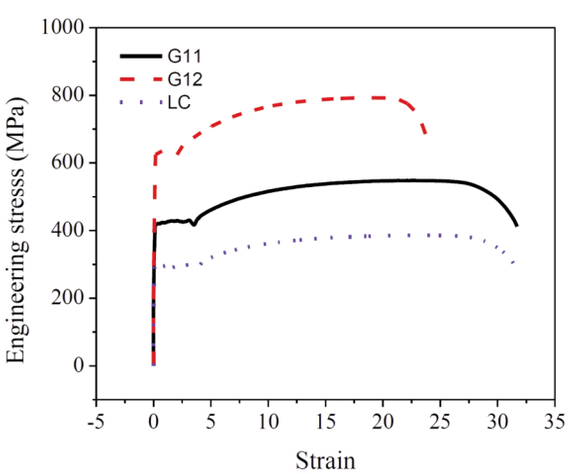

Figure 5. *Engineering stress-strain curve of as rolled specimens G11, G12 and LC*

Table 2. *Tensile properties of as rolled specimen G11 and G12 at room temperature.*

Sample	Average Yield Strength (Mpa)	Average UTS (Mpa)	Percentage elongation
G11	370.0 ± 5.0	546.0 ± 2.0	28.0 ± 3.0
G12	551.0 ± 25.0	708 ± 30.0	24.0 ± 1.0
LC	287 ± 14.0	379 ± 14.0	30.0 ± 4.0

percentage elongation at fracture indicate standard deviation.

This deviation is expected due to the microstructural inhomogeneity of steels. As shown in Fig. 4 and 5, the yield stress and ultimate tensile stress of the specimens increase and the percentage of elongation at fracture decreases on increasing phosphorus content. The higher values of YS and UTS of G12 steel indicate strong solid solution strengthening effect of phosphorus. The atomic radius of phosphorus is 1.1 Å and that of iron is 1.24 Å. When phosphorus is present in solid solution in ferrite it severely distorts the crystal lattice and leads to increase in YS, UTS and decrease in % of elongation [22-24]. Therefore, while the ductility of high phosphorus containing steels G11 and G12 is comparable with that of the low carbon steel (LC), both YS and UTS are much higher than that of LC. This will be further understood from the fractography of fractured samples in the following section.

SEM fractographs of test specimen G11 (Fig. 7a & b) show primarily ductile dimple rupture. The dimples are conical equiaxed, along with some elliptical & elongated cup and cone depressions, which is generally expected for ductile material that fails under uniaxial tension [25]. These types of ductile fracture are due to the formation and coalescence of micro voids. The white arrow in Fig. 7 (a) is attributed to the ductile crack growth due to growth of voids in crack tips. The higher magnification fractrographs in Fig. 7

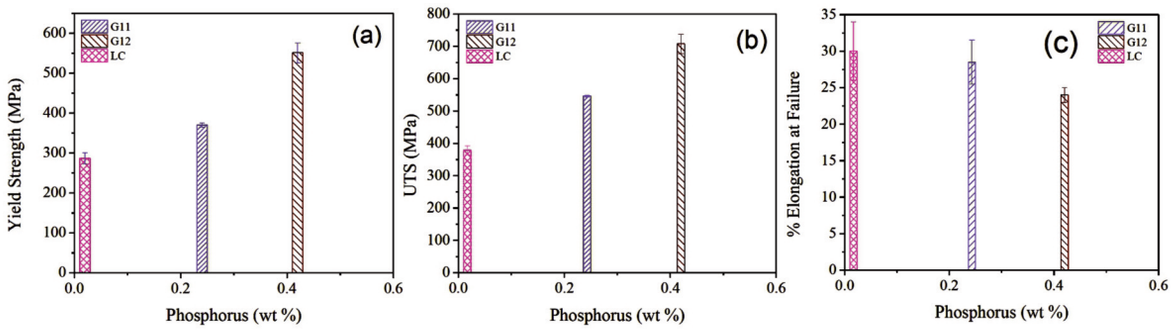

Figure 6. *Average values of mechanical properties, (a) Yield strength, (b) UTS and (c) percentage elongation at fracture of as rolled specimens G11, G12 and LC*

(b & d) indicate that the density of micro voids is higher in G11 than that of higher phosphorus containing G12. As cleavage is a characteristic of transgranular brittle fracture [25], the presence of some cleavage fractures as indicated by arrow in Fig. 7(b) of G11 steel shows that phosphorus is probably impairing ductility of the material. The close examination of fractured surface of G12 (Fig. 7 (c & d)) reveals the presence of cleavage fracture facets in large ferrite grain along with few conical dimples, which will be resolved at higher magnification. Therefore, the higher ductility of G11 and LC steel and lower ductility of G12 steel has been replicated in fractographs shown in Fig. 7 in the form of mode of fractures. The pancake shaped grains of G12 steel, as observed in Fig. 2 (b) and 3 (c & d), has been also replicated in Fig. 7 (c & d) as elongated cleavage fracture facets. The fracture mode has been changed to almost 100 % cleavage fractures on increasing phosphorus content from 0.25% to 0.42%. Furthermore, the fractograph shows that pancake shaped or textured steel is attainable on increasing phosphorus content in steel.

Impact strength depends on structure of metal. Coarse grains of the metal substantially reduce the impact strength [26]. The CVN energy result of the test samples shows reduction in impact energy in coarse grained and high P G12 steel, which is 4 Joule while that of G11 steel is 32 Joule. While decrease in grain size is one of the important factor in increasing toughness of the materials, segregation of P to the grain boundary is well known for decreasing CVN energy of steel as the reported CVN energy of low carbon and low alloy steel at RT is more than 100 J. As carbon also decreases CVN energy, pearlitic rail steel has CVN energy below 20 Joule [27]. Out of both G11 and G12 steel, the former qualifies the minimum requirement of 27 J at 20^{o}C for some structural applications viz. S235JR, S275JR, S335JR grade steels of CSN EN 10025-2: 2004 specification, where 235, 275 and 335 indicates minimum yield strength [28]. The sufficient ductility (percentage elongation equal to 28.0 ± 3.0) and fulfillment of required CVN energy of G11 steel having reasonably higher amounts of phosphorus (0.25%) for the above grade steel is partly attributed to the effect of free boron present in the steel, which replaces phosphorus from the grain boundary [15-17]. As aluminum has been added to the experimental steels to tie up with nitrogen, the ferrite region in Fig.4(b) shows AlN phase. The free boron in the form of Fe_2B and its estimated concentration has been determined by the compositional analysis using FactSage software. At 250^{0}C temperature in Fig. 4b, the estimated amount of BN is found to be zero while that of AlN and Fe_2B are 0.0146% and 0.025%, respectively for both G11 and G12 steels. However, the effect of boron may not be sufficient to reduce completely the grain boundary segregation effect of phosphorus as, even 0.25% of phosphorus is also very high. This may be one of the reason for impairing ductility and the grain boundary decohesion, which is further evident below in the discussion from the fractorgraphy of CVN tested sample.

SEM fractographs of test specimens G11 in (Fig. 8a & b) and that of G12 (Fig. 8c & d) reveal bright and granular fractographic view in lower magnification, which is an indicative of cleavage fracture. Phosphorus produces marked work hardening in iron when cold worked. This promotes cleavage fracture and thus increases the likelihood of brittle fracture [29].

The characteristic feature of cleavage fracture is flat facets which are generally about the size of ferrite grains of the alloy steel. The facets in Fig. 8 (b & d) exhibit some river markings. Few decohesive ruptures (locations marked by arrows) are also noticed for G11 and G12 at higher magnifications (Fig. 8). In addition to work hardening effect of phosphorus, it has a well known tendency to segregate to the grain boundary, which may drastically reduce cohesive strength and hence lower CVN energy.

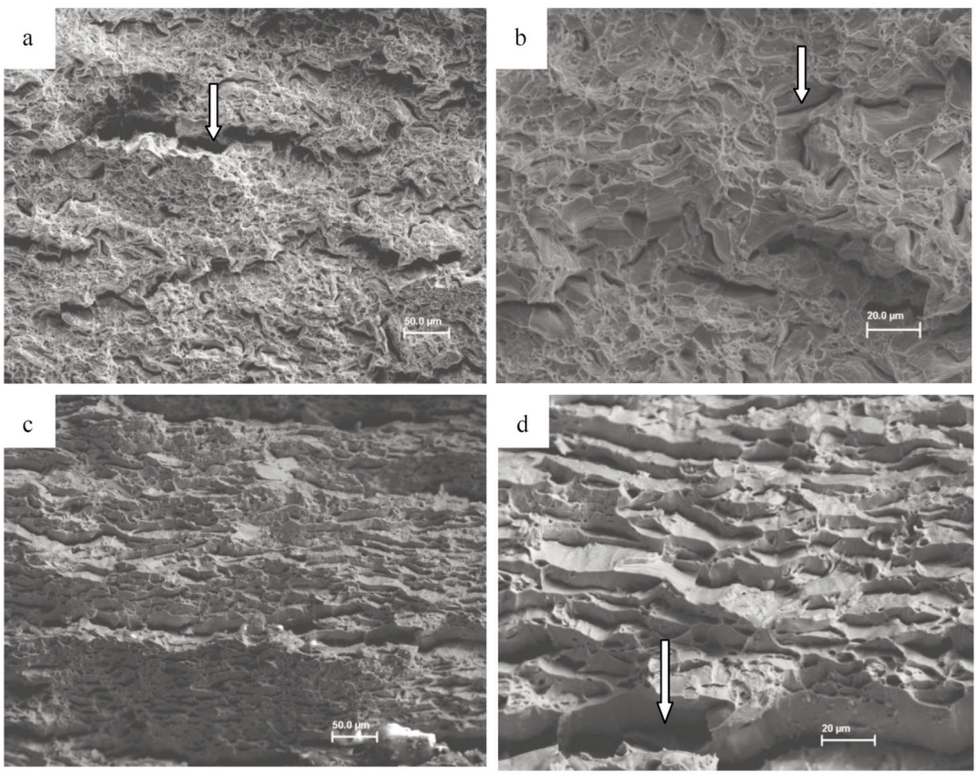

Figure 7. *Fractographs after tensile test in lower and higher magnification of as received G11 (a & b) reveal primarily dimple fracture and G12 (c &d) reveal cleavage rupture with some dimples.*

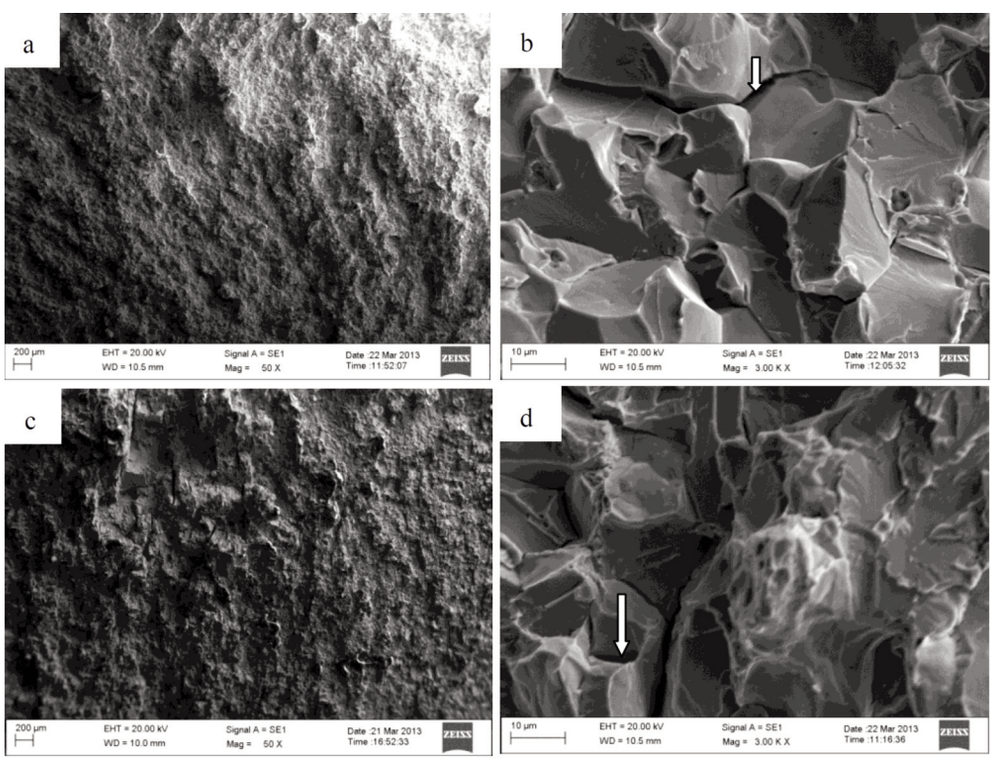

Figure 8. *SEM fractographs of CVN impact test specimens G11 (a & b) and G12 (c &d) at lower and higher magnifications with decohesive ruptures marked by arrows*

4. Conclusions

SEM and light optical microscopy examination of both G11 and G12 steel revealed ferrite and pearlite microstructure and grain size increased with increasing phosphorus content.

Phosphorus markedly influenced morphology of grain which changed from equiaxed shape to pancake shape on increasing phosphorus content from 0.25% to 0.42%.

The engineering stress-strain curves of G11 and G12 steel indicated yield point phenomenon with % of elongation at fracture greater than 24 %.

The solid solution strengthening of phosphorus in G11 and G12 was established from the observed increasing trend of YS and UTS and decreasing trend of ductility on increasing phosphorus content.

SEM fractographs of tensile specimen indicated primarily ductile mode of fracture with micro void coalescence in G11 steel while G12 steel revealed transgranular cleavage fracture.

The presence of high amount of phosphorus in G11 and G12 steel decreased CVN energy drastically, which is attributed to the decrease in cohesive energy of the material.

Acknowledgement

Authors are very much thankful to the management of R & D Centre for Iron and Steel, SAIL, Ranchi for providing the necessary support to carry out this work. Authors are also thankful to the corresponding laboratory personnel for their full support and help in conducting experiments.

References

[1] H.E. Townsend, T.C. Simpson and G.L. Johnson, Corrosion 50 (1994) 546-554.

[2] M. Morcillo, B. Chico, I. Díaz, H. Cano and D. de la Fuente, Corros. Sci., 77 (2013) 6-24.

[3] Ch. Thee, L. Hao, J. Dong, X. Mu, X. Wei, X. Li and W. Ke, Corros. Sci., 78 (2014) 130-137.

[4] B.R. De Meybaum and E. S. Ayllon, Corrosion 36 (1980) 345-347.

[5] Y.S. Choi, J.J Shim and J.K. Kim, Mater. Sci. Engg. 385A (2004) 148-156.

[6] R. Balasubramaniam, Corros. Sci. 42 (2000) 2103-2129.

[7] R. Balasubramaniam and A.V. Ramesh Kumar, Corros. Sci, 42 (2000) 2085-2101.

[8] G.P. Zhou, Z.Y. Liu, Y.Q. Qiu and G.D. Wang, Mater Design. 30 (2009) 4342–4347.

[9] S.K. Banerji, C.J. McMahon, and H.C. Feng, Metall. Trans. A. 9A (1978) 237-247.

[10] C.L. Briant, and S.K. Banerji, Metall. Trans. A. 10A (1979) 123-126.

[11] C.L. Briant, and S.K. Banerji, Metall. Trans A. 13 (1982) 827-836.

[12] W. Steven and K. Balajiva, J Iron Steel Inst. 193 (1959) 141-147.

[13] K. Abiko, S. Suzuki, and H. Kimura, T Jpn I Met. 23 (1982) 43-52.

[14] S. Suzuki, K. Abiko, and H. Kimura, T Iron Steel I Jpn. 25 (1985) 62-68.

[15] Wu Ruqian, A.J. Freeman and G.B. Olson, Sci. 265 (1994) 376.

[16] M. I. Haq and N. Ikram, J. Mater. Sci. 28 (1993) 5981-5985.

[17] C.M. Liu, T. Nagoya, K. Abiko and H. Kimura, Metall. Trans. 23A (1992) 263-269.

[18] ASTM E 8M-98, "Standard test Methods for flat bar tensile testing of metallic materials"

[19] ASTM E 23-05, "Standard test Methods for Impact Testing of metallic materials"

[20] G. Sahoo and R. Balasubramaniam, Metall. Trans. 38A (2007) 1692-1697.

[21] G.E. Dieter, Mechanical Metallurgy, SI Metric Edition, McGraw-Hill Book Company, New York, (1988) 197 and 478.

[22] B.E. Hopkins, and H.R. Tipler, J Iron Steel Inst. 188 (1958) 218-237.

[23] W.A. Spitzig, Metall. Trans. 3 (1972) 1183-1188.

[24] W.A. Spitzig, Mater. Sci. Engg. 16 (1974) 169-179.

[25] V. Kerlins, in ASM hand book (J. R. Davis & J. D Destefani), Vol. 12, Fractography, ASM International, Materials Information Society, USA, 1999, p.12-14.

[26] Y. Lakhtin, Engineering Physical Metallurgy, Mir Publisher, Moscow, 1977, p.85.

[27] H. Yokoyama, S. Mitao, S. Yamamoto, Y. Kataoka and T. Sugiyama, High Strength Bainitic Steel Rails for Heavy Haul Railways with Superior Damage Resistance, NKK Technical Review No. 84 (2001) 44-51.

[28] European Standard No. CSN EN 10025-2: 2004, Hot rolled products of structural steels - Part 2: Technical delivery conditions for non-alloy structural steels

[29] Y.Q. Weng, and C.J. Mcmahon, Mater. Sci. Tech. 3 (1987) 207-216.